DISTRIBUTION STATEMENT A. Approved for public release; distribution is unlimited.

Three-Dimensional Scale-Model Tank Experiment of the Hudson Canyon Region

Jason D. Sagers
Applied Research Laboratories at The University of Texas at Austin
Environmental Science Laboratory
Austin, TX 78758
phone: (512) 835-3195 fax: (512) 490-4225 email: sagers@arlut.utexas.edu

Award Number: N00014-13-1-0109

LONG-TERM GOALS

The long-term scientific goal of this project is to advance understanding of three-dimensional (3D) acoustic propagation in range-dependent ocean waveguides by studying propagation in a scale-model laboratory environment.

OBJECTIVES

The objective of this work is to generate high quality acoustic data, measured in the laboratory, that will (1) provide a benchmark standard for 3D numerical models currently being developed, (2) allow researchers to carefully investigate 3D acoustic propagation in a controlled waveguide, and (3) assist ONR in planning for future experiments in ocean environments with slopes and canyons.

APPROACH

The development of fully 3D numerical acoustic propagation models is an area of ongoing research.[1–7] These models have the potential to be very accurate, but comparisons between data taken at sea and numerical predictions often suffer because of insufficient environmental inputs to the numerical model. This is already a problem for two-dimensional (2D) data-model comparisons and is a significantly greater problem when trying to employ 3D numerical models to describe experimental data.

An alternative way to provide benchmark-quality data for numerical models is to conduct physical scale-model laboratory experiments. Scale-model experiments permit tight control over many of the variables affecting acoustic propagation, such as water temperature, bathymetry, source/receiver geometry, surface and seafloor roughness, and the geoacoustic properties of the modeled seafloor. Control over these variables allow for precise observation of 3D acoustic propagation effects such as horizontal refraction, shadow zones, multiple mode arrivals, and intra-mode interference.

Figure 1 illustrates the technical approach. The scale-model bathymetry is suspended below the air-water interface of an indoor test tank on a mechanical support structure. An acoustic source is positioned at a fixed point in space and broadcasts acoustic signals. A computer-controlled positioning system accurately locates the receiving hydrophone in three-dimensional space. An acoustic I/O system

both generates the acoustic source signal and digitally acquires the acoustic data at the receiver. High quality acoustic data are acquired for various user-defined source and receiver positions over the scale model. High spatial sampling of the acoustic field could allow for data post-processing that includes both horizontal and vertical beamforming. Auxiliary measurements (such as water temperature and receiver position) are also recorded.

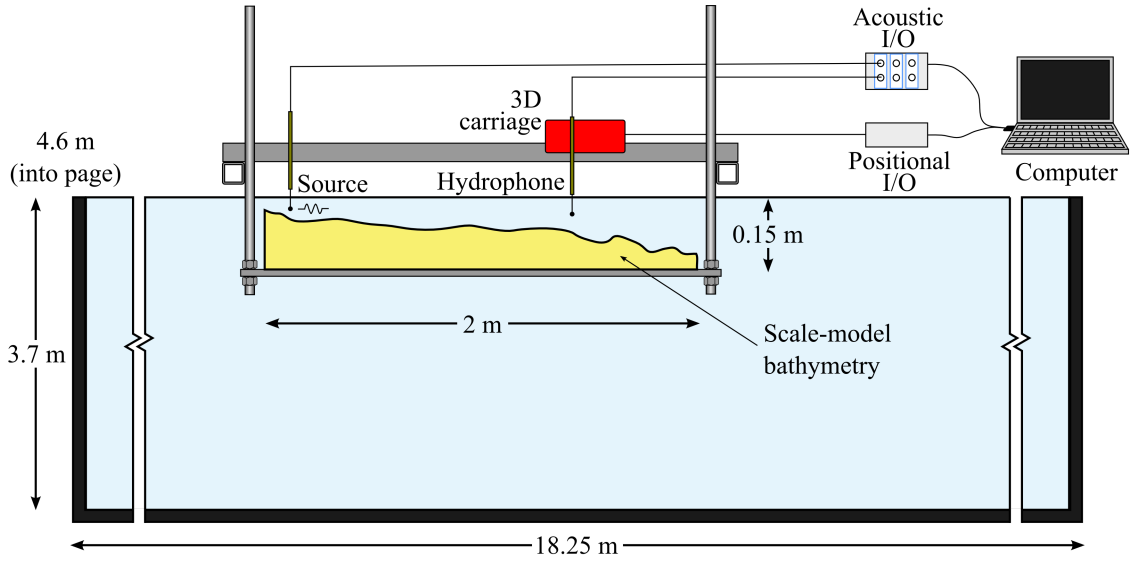

Figure 1: Illustration showing the experimental apparatus.

WORK COMPLETED

The work completed during FY14 includes the items listed below. The progress in each of these areas is discussed in the Results section.

1. Fabrication of the mechanical support structure and installation of the computer-controlled positioning system.
2. Development of the LabVIEW control software.
3. Calibration of the acoustical transducers.
4. Construction and installation of the calibration bathymetry.
5. Initiation of the acoustic measurements and data analysis.

RESULTS

1. Mechanical support structure and positioning system

A computer-aided design (CAD) model of the experimental apparatus is shown in Fig. 2(a) and a photograph of the completed apparatus installed in the indoor tank room at ARL:UT is shown in Fig. 2(b). The major components of the apparatus include the rigid mechanical frame, the linear stages and stepper motors which comprise the computer-controlled positioning system, the acoustic

(a) CAD model

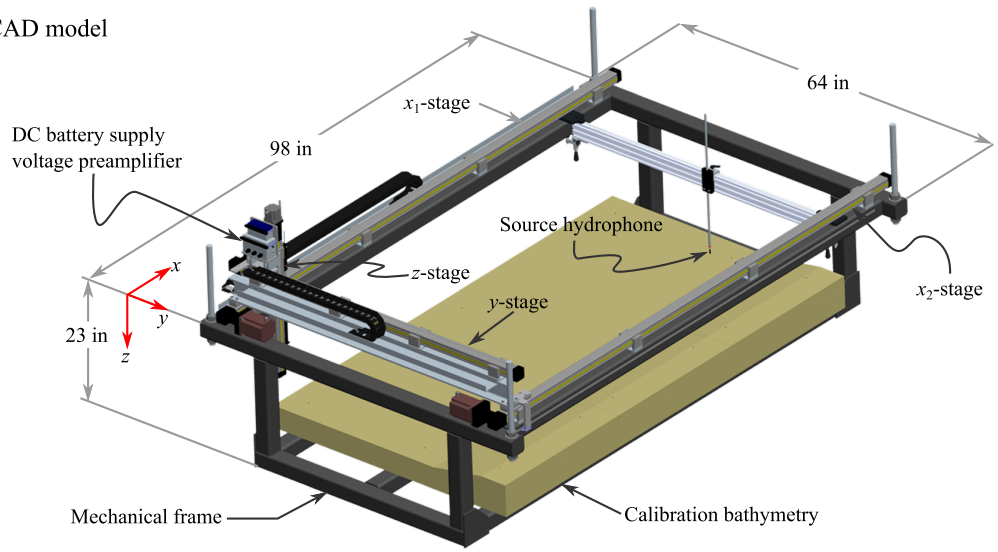

(b) Photograph in ARL:UT indoor tank room

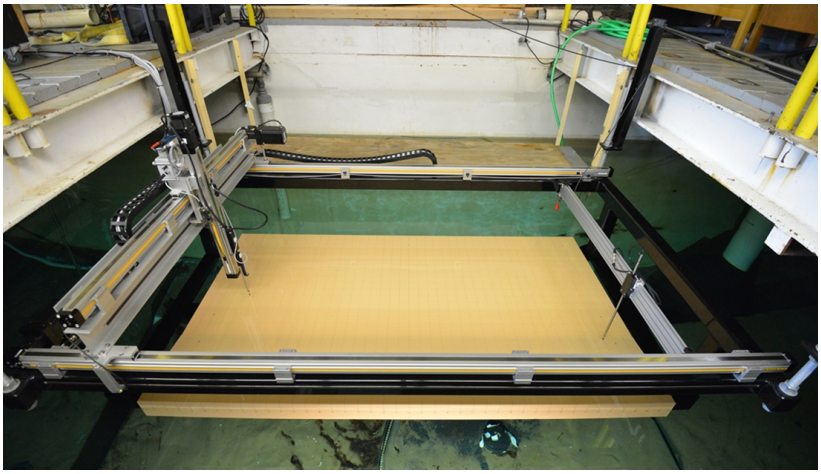

Figure 2: (a) CAD model of the experimental apparatus, and (b) photograph of the apparatus installed in the ARL:UT indoor tank room.

transducers, and the calibration bathymetry. The rigid frame is constructed from 3" square structural steel tubing that has been welded together and then powder-coated to provide corrosion resistance when submerged. The x_1 and x_2 belt-driven, linear stages are affixed to the top surface of the rigid frame. The y-stage is affixed to the two x-stage carriages, and the z-stage is affixed to the y-stage carriage. The cabling for the stepper motors, linear encoders, and hydrophones is bundled and routed back to the computer control center.

The bathymetric part is affixed to the rigid frame by bolts which are accessible from underneath the apparatus. The receiving hydrophone is affixed at the bottom end of the z-stage and can be positioned by the computer to an accuracy of 0.002" in all three Cartesian directions. The voltage preamplifier and requisite D/C battery power supply are affixed atop the y-stage carriage. The source transducer is attached to a manually-positioned rail which clamps to the rigid frame and can be positioned to an accuracy of approximately 0.050".

2. LabVIEW control software

A custom LabVIEW application was written to automate the measurement process. The important functionality of the software includes a positional registration routine, the ability to define scan point files, and the prescription of the acoustic measurement parameters (such as waveform type, sampling frequency, etc.). The data collection process is entirely automated after the measurement is configured and initiated.

3. Transducer calibration

Acoustical calibration of the source and receiving hydrophones is important because the objective of the current work is to provide benchmark quality data to the modeling community. A through-the-system (TTS) calibration was conducted to account for the non-ideal transmit sensitivity, receive sensitivity, vertical directivity, and voltage preamplifier. The inclusion of the frequency-dependent vertical directivity in the calibration is particularly important so that energy from the vertical multipath propagation is properly scaled in a numerical model.

4. Calibration bathymetry

An 84" long (x-direction) by 48" wide (y-direction) *calibration bathymetry* was fabricated for the initial set of acoustic measurements. The calibration bathymetry consists largely of a range-independent region with a translationally invariant wedge of 10° slope on one edge [c.f. Fig. 3(b)]. Because of manufacturing considerations, the slope does not come to a perfect taper at its deepest point (defined by the line y = 32.3"), but instead has a 0.040" step discontinuity at the edge. The bathymetric part was fabricated from Renshape 5030, which is a commercially available closed-cell polyurethane machining board, whose ultrasonic reflection coefficient was previously measured.[8] Several 5 mm diameter stainless steel pins were embedded at known positions around the perimeter of the calibration bathymetry. An induction proximity sensor, attached to the z-stage, automatically locates these pins as part of the positional registration procedure.

5. Acoustic measurements and data analysis

This section describes three acoustic measurements made with the calibration bathymetry where the water depth of the large range-independent section was set at 3.5". The layout for two of the experiments is depicted in Fig. 3. In the first experiment, the acoustic center of the source hydrophone was located at (x,y,z) = (68,18,3) inches. A 3" high (241 element) synthetic vertical line array (VLA) was centered at (x,y) = (42,18) inches and a 4" wide (321 element) synthetic horizontal line array (HLA) was centered at (x,y,z) = (42,18,3) inches. The source waveform was a 50 μs LFM chirp with 1 MHz center frequency and 2 MHz bandwidth.

Post-processing involved cross-correlating the source waveform with the recorded waveform from each array element, and then applying a time-domain beamformer to the cross-correlated result. The beamfored results for the VLA and HLA are shown in Figs. 4(a) and (b), respectively. The vertical multipath arrivals on the horizontal beam looking directly at the source are visible at 0° on the HLA display, and sweep out a parabola on the VLA display with the vertical energy alternating between upward- and downward-going arrivals. The source depth and VLA phase center are located at z = 3", so the vertical multipath arrivals in Fig. 4(a) are not symmetric about 0°. Between about 730 and 1000 μs, a group of arrivals comes in between 25° to 50° relative to broadside on the HLA. These arrivals are due to acoustic scattering from the step discontinuity at the base of the wedge. Energy that has undergone horizontal refraction from the slope arrives between 1200 and 1400 μs at horizontal angles between 30°

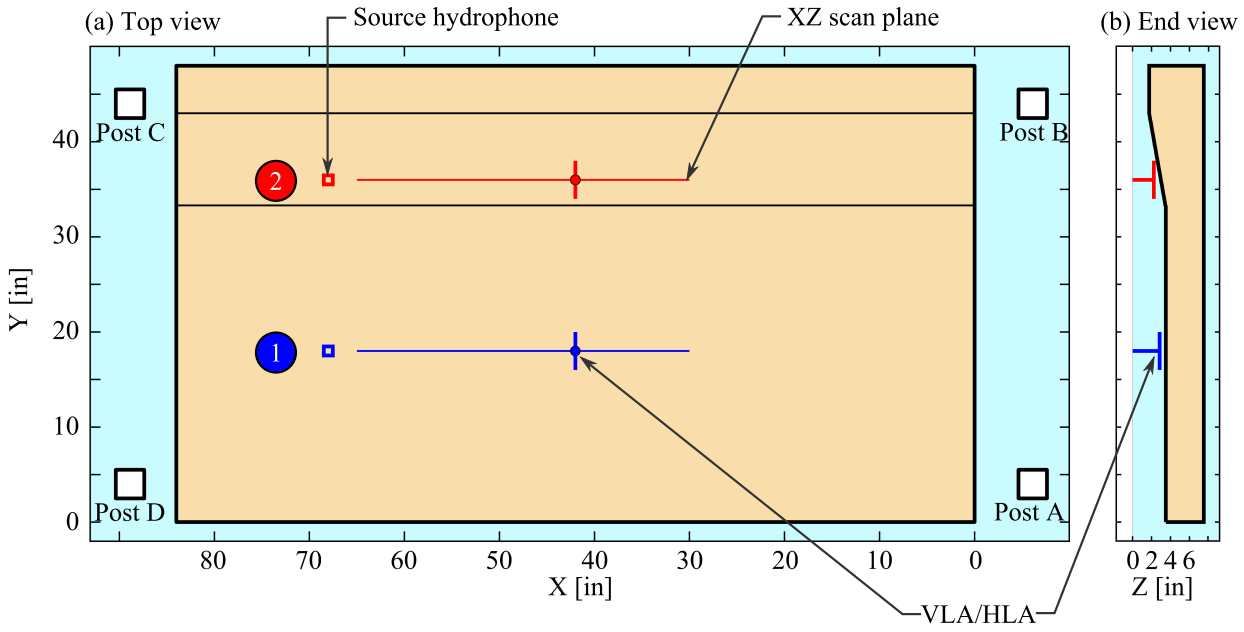

Figure 3: (a) Top view and (b) end view of two propagation experiments conducted with the calibration bathymetry.

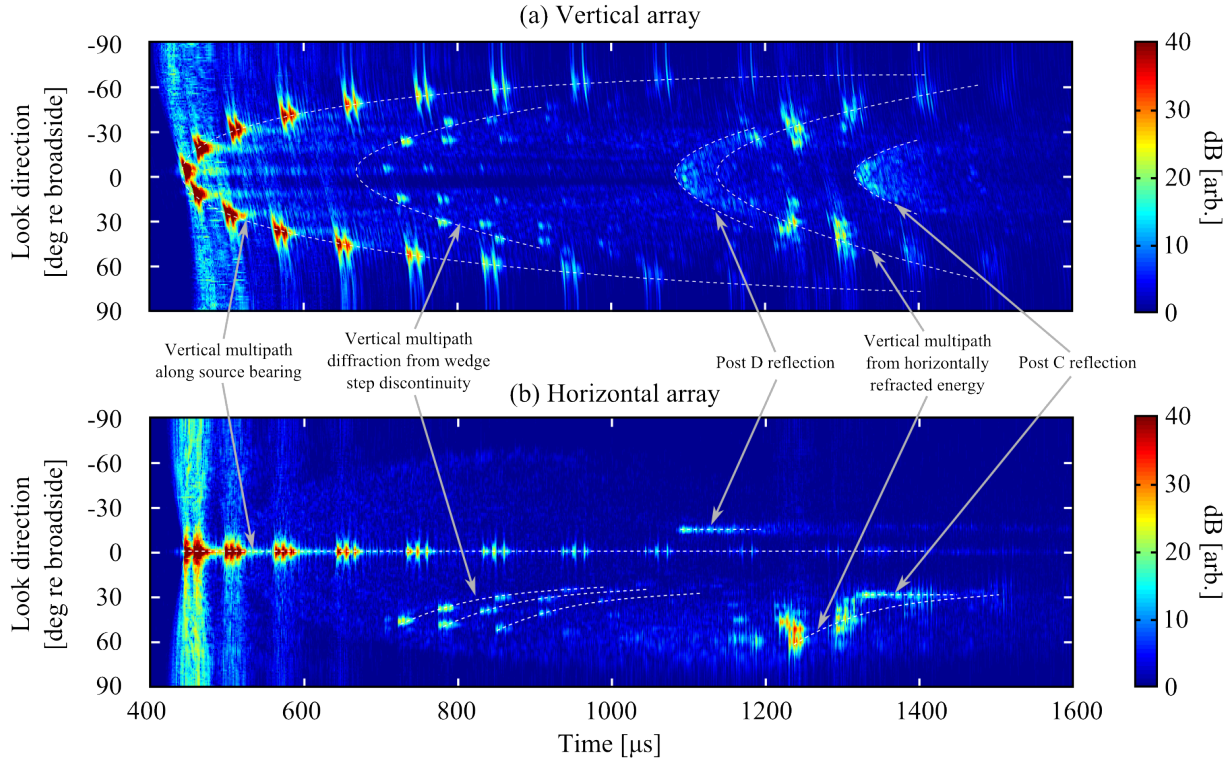

Figure 4: (a) Vertical and (b) horizontal beamforming display for the first propagation experiment. Dashed lines have been added to help identify the various arrival types.

and 60°. Finally, two acoustic reflections from vertical posts D and C are visible on the HLA display at 1092 μs and -16°, and 1330 μs and 28°, respectively. The corresponding vertical angles are also visible on the VLA display.

For the second experiment, the source and receiver positions were translated to y = 36" and the source/receiver depth was raised to 2.25" to avoid intersection with the sloping bathymetry. The beamformed results for the VLA and HLA are shown in Figs. 5(a) and (b), respectively. Of significant note is the lack of vertical multipath arrivals along the source beam due to horizontal refraction of the bottom-interacting energy. For the same physical reason, the steepening vertical arrivals come in with increasing horizontal angles between 450 and 720 μs on the HLA display. There are two distinct arrival paths visible in the HLA display which have a relative offset of approximately 10°, corresponding to one additional bottom interaction. One also notes the lack of scattered energy from the step discontinuity for this experimental geometry. The hypothesis is that the amount of backscattered energy is substantially less when *stepping down* the discontinuity than in the *step up* geometry. Two acoustic reflections from posts C and D are visible at 1031 μs and 6°, and 1450 μs and -35°, respectively.

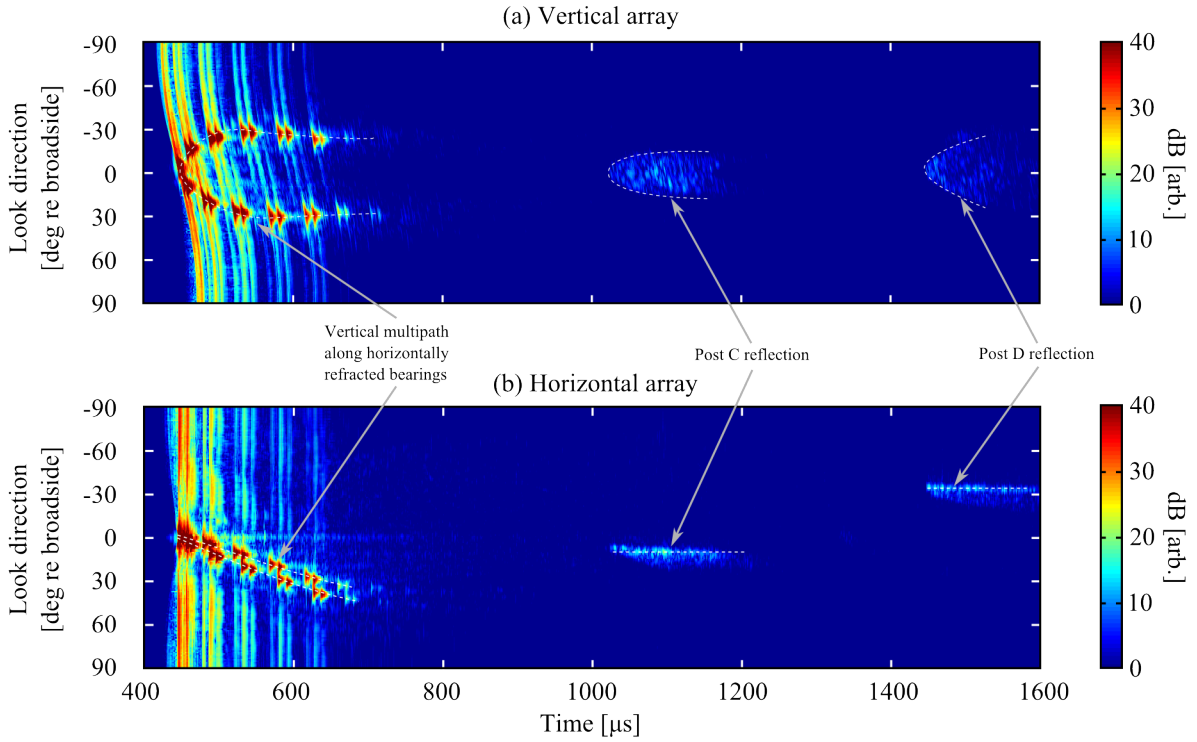

Figure 5: (a) Vertical and (b) horizontal beamforming display for the second propagation experiment. Dashed lines have been added to help identify the various arrival types.

The third experiment was a planar scan at a receiver depth of 0.10" with the source located at (x,y,z) = (68,25,2.25) inches. The intensity at a time snapshot of 747 μs is shown in Fig. 6. The non-bottom-interacting cylindrically spreading wavefront is clearly visible at the far right. Each wavefront to its left has had one or more bottom interactions. Horizontally refracted wavefronts are clearly visible in the region of the slope. A close inspection of the figure also reveals a few wavefronts that were generated from scattering at the step discontinuity of the slope.

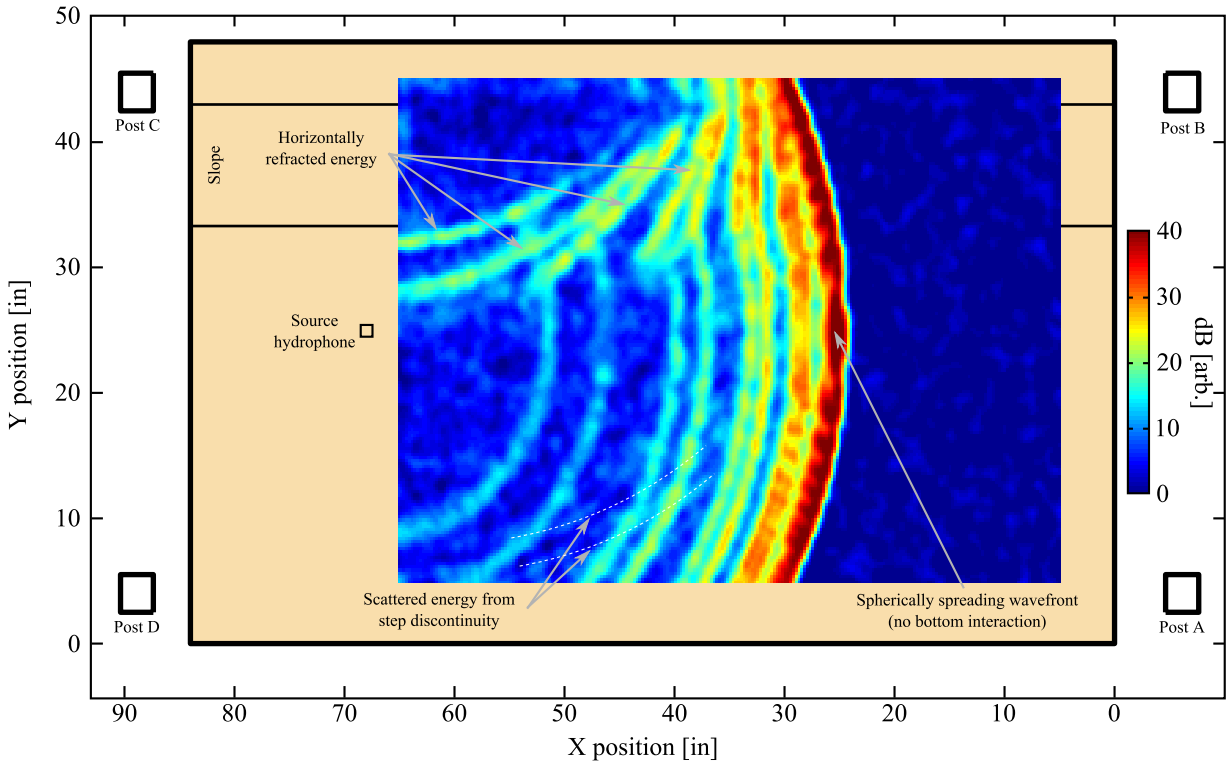

Figure 6: Planar scan at depth z = 0.10" at time 747 μs showing 3D propagation effects.

IMPACT/APPLICATIONS

The impact of this research is to understand the importance of 3D acoustic propagation induced by bathymetric features and to provide a benchmarking opportunity to newly developed acoustic propagation models.

TRANSITIONS

The primary transition for this project is to make direct analysis of the 3D propagation effects and to make available the experimental data to principal investigators who develop numerical propagation models. Comparisons to 3D numerical modeling have already begun with Dr. Megan Ballard of ARL:UT.

RELATED PROJECTS

Recently recovered acoustic data from the Gulf of Mexico were investigated for evidence of 3D acoustic propagation. Analysis of the measured acoustic data suggests that horizontal refraction from canyon walls occurs for certain source ranges. A JASA manuscript has been accepted and is scheduled for publication in November 2014.

Recently recovered acoustic data from the Gulf of Oman were also investigated within a statistical inference methodology to infer information about seabed properties.

REFERENCES

[1] M. J. Buckingham, "Theory of three-dimensional acoustic propagation in a wedgelike ocean with a penetrable bottom," J. Acoust. Soc. Am. **82**, 198–210 (1987).

[2] M. D. Collins and S. A. Chin-Bing, "A three-dimensional parabolic equation model that includes the effects of rough boundaries," J. Acoust. Soc. Am. **87**, 1104–1109 (1990).

[3] D. Lee, G. Botseas, and W. L. Siegmann, "Examination of three-dimensional effects using a propagation model with azimuth-coupling capability (FOR3D)," J. Acoust. Soc. Am. **91**, 3192–3202 (1992).

[4] J. Fawcett, "Modeling three-dimensional propagation in an oceanic wedge using parabolic equation methods," J. Acoust. Soc. Am. **93**, 2627–2632 (1993).

[5] G. B. Deane and M. J. Buckingham, "An analysis of the three-dimensional sound field in a penetrable wedge with a stratified fluid or elastic basement," J. Acoust. Soc. Am. **93**, 1319–1328 (1993).

[6] K. B. Smith, "A three-dimensional propagation algorithm using finite azimuthal aperture," J. Acoust. Soc. Am. **106**, 3231–3239 (1999).

[7] M. S. Ballard, Y. T. Lin, and J. F. Lynch, "Horizontal refraction of propagating sound due to seafloor scours over a range-dependent layered bottom on the New Jersey shelf," J. Acoust. Soc. Am. **131**, 2587–2598 (2012).

[8] J. D. Sagers, M. R. Haberman, and P. S. Wilson, "Ultrasonic measurements of the reflection coefficient at a water/polyurethane foam interface," J. Acoust. Soc. Am. **134**, EL271–EL275 (2013).

PUBLICATIONS

Peer-reviewed papers

J. D. Sagers, M. S. Ballard, and D. P. Knobles, "Evidence of three-dimensional acoustic propagation in the Catoche Tongue," J. Acoust. Soc. Am., [in press, refereed].

J. D. Sagers and D. P. Knobles, "Statistical inference of seabed sound-speed structure in the Gulf of Oman Basin," J. Acoust. Soc. Am. **135**, 3327-3337 (2014) [published, refereed].

A. R. McNeese, P. S. Wilson, J. D. Sagers, and P. S. Wilson, "An impulsive source with variable output and stable bandwidth for underwater acoustic experiments," J. Acoust. Soc. Am. **136**, EL8-EL12 (2014) [published, refereed].

D. P. Knobles and J. D. Sagers, "Forward and backward modal statistics for rough surface scattering in shallow water," J. Comp. Aco. **22**, 144004 (2014) [published, refereed].

J. D. Sagers, M. R. Haberman, and P. S. Wilson, "Ultrasonic measurements of the reflection coefficient at a water/polyurethane foam interface," J. Acoust. Soc. Am. **134**, EL271-EL275 (2013) [published, refereed].

Technical reports

J. D. Sagers, "Ultrasonic attenuation and deflection panels," Technical Report ARL-TL-EV-14-80, Applied Research Laboratories (2014).

J. D. Sagers, A. P. Hill, M. R. Haberman, and P. S. Wilson, "Ultrasonic reflection coefficient measurement (RCM) apparatus," Technical Report ARL-TL-EV-13-72, Applied Research Laboratories (2013).

Conference presentations

J. D. Sagers and D. P. Knobles, "Statistical inference of seabed sound-speed structure in the Gulf of Oman Basin," J. Acoust. Soc. Am. **135**, 2301 (2014).

R. D. Lenhart, J. D. Sagers, and P. S. Wilson, "Development of a standing-wave calibration apparatus for acoustic vector sensors," J. Acoust. Soc. Am. **135**, 2396 (2014).

M. S. Ballard and J. D. Sagers, "Explanation of an extended arrival structure measured in the Catoche Tongue using a three-dimensional propagation model," J. Acoust. Soc. Am. **135**, 2429 (2014).

D. P. Knobles and J. D. Sagers,"Influence of rough seabed surface on statistics of modal energy flux," J. Acoust. Soc. Am. **133**, 3252 (2013).